Single crystal growth, structure and magnetic properties of $Pr_2Hf_2O_7$ pyrochlore

2017 J. Phys.: Condens. Matter 29 075902

(http://iopscience.iop.org/0953-8984/29/7/075902)

IOP Publishing Journal of Physics: Condensed Matter
J. Phys.: Condens. Matter **29** (2017) 075902 (9pp) doi:10.1088/1361-648X/29/7/075902

Single crystal growth, structure and magnetic properties of $Pr_2Hf_2O_7$ pyrochlore

Monica Ciomaga Hatnean[1], Romain Sibille[2], Martin R Lees[1], Michel Kenzelmann[2], Voraksmy Ban[3], Vladimir Pomjakushin[4] and Geetha Balakrishnan[1]

[1] Department of Physics, University of Warwick, Coventry, CV4 7AL, UK
[2] Laboratory for Scientific Developments and Novel Materials, Paul Scherrer Institut, 5232 Villigen PSI, Switzerland
[3] Laboratory for Synchrotron Radiation—Condensed Matter, Paul Scherrer Institut, 5232 Villigen PSI, Switzerland
[4] Laboratory for Neutron Scattering and Imaging, Paul Scherrer Institut, 5232 Villigen PSI, Switzerland

E-mail: M.Ciomaga-Hatnean@warwick.ac.uk and romain.sibille@psi.ch

Received 21 September 2016, revised 27 October 2016
Accepted for publication 10 November 2016
Published 29 December 2016

Abstract

Large single crystals of pyrochlore $Pr_2Hf_2O_7$ were successfully grown by the floating zone technique using an optical furnace equipped with high power xenon arc lamps. Structural investigations were carried out via powder synchrotron x-ray and neutron diffraction to establish the crystallographic structure of the materials produced. The magnetic properties of the single crystals were determined for magnetic fields applied along different crystallographic axes. The results revealed that $Pr_2Hf_2O_7$ is an interesting material for further investigation as a frustrated magnet. The high quality of the crystals produced makes them ideal for detailed investigation, especially using neutron scattering techniques.

Keywords: floating zone crystal growth, pyrochlore, geometrically frustrated magnetism, quantum spin ice, hafnates, praseodymium based pyrochlore

(Some figures may appear in colour only in the online journal)

1. Introduction

Pyrochlore oxides are a topic of great interest because of the intriguing magnetic properties that originate from their frustrated magnetic lattice [1–7]. Pyrochlores are compounds of the general formula $A_2B_2O_7$ (where A and B are metals) and have a face-centred cubic structure with space group $Fd\bar{3}m$ (no. 227). The majority of pyrochlore oxides belong to the (3+, 4+) type $A_2^{3+}B_2^{4+}O_7$, where the A sites are occupied by trivalent cations located in the centre of scalenohedra (distorted cubes) of oxygen anions, and the B sites are occupied by tetravalent transition metal ions situated in the centre of oxygen octahedra [8]. A and B cations form, independently, two so-called pyrochlore lattices of corner-sharing tetrahedra [3, 4]. Depending on the nature and strength of the magnetic moment and interactions, pyrochlore oxides can display a wide variety of magnetic ground states [4], ranging from spin ice [2, 9, 10], where the spin correlations lead to a Coulomb phase [11, 12] with emergent magnetostatics [13, 14], through spin frozen states [15–17], to long-range ordered states (see [4] and references therein).

In addition, one of the most intriguing areas of current research concerns materials which exhibit quantum spin liquid (QSL) ground states, as has been pointed out in recent studies on pyrochlores based on Yb^{3+} [18–20] (although this case is under debate [21, 22]), Pr^{3+} [23–27] and Ce^{3+} [28]. The candidate materials for the realization of QSL states are based on rare-earth ions that develop relatively small magnetic moments. The reason for this is that, for small magnetic moments, the transverse terms in the effective spin −1/2 Hamiltonian on the pyrochlore lattice [18, 29], which are responsible for the stabilization of quantum phases [7, 24, 30–32], are not overwhelmed by the dipolar interaction that leads to classical spin ice when the dipolar interaction dominates.

The synthesis of large, high quality single crystals of pyrochlore oxides, and in particular rare-earth titanates [33–35]

and some rare-earth molybdates [36, 37] and zirconates [24] [38–40] has been accomplished using the floating-zone technique. This success has allowed real and rapid progress to be made in the investigation of frustrated magnets, with some very interesting magnetic properties being unearthed. All the members of the titanate pyrochlore family have been thoroughly investigated in recent years, while the molybdate [36, 37, 41, 42] and zirconate [24, 27, 38, 43, 44] series have only recently come to the attention of the research community. Recent studies have reported on the availability of large crystals of the frustrated pyrochlore magnet $Nd_2Hf_2O_7$ [45]. The floating zone technique is ideal to produce crystals of other members of the rare-earth hafnate pyrochlores. This is particularly appealing, since the structural and magnetic characteristics of the hafnate family have not yet been investigated in great detail.

Recent studies of the intriguing magnetic properties of the praseodymium based pyrochlores $Pr_2Zr_2O_7$ [27] and $Pr_2Ir_2O_7$ [46] motivated us to embark upon the study of the analogous compound in the hafnate pyrochlore series, $Pr_2Hf_2O_7$. We succeeded in preparing, for the first time, single crystals of praseodymium hafnate pyrochlore using the floating-zone technique. The growth of large high quality single crystals of this oxide represents an important step in the field, and opens up a route to further investigation of this novel class of pyrochlores, with the potential to lead to an in-depth understanding of the effects of frustration in praseodymium containing pyrochlores [25]. In this paper, we report the synthesis, structural characterization and preliminary study of the magnetic properties of single crystals of praseodymium hafnate pyrochlore, $Pr_2Hf_2O_7$.

2. Experimental section

Polycrystalline samples of $Pr_2Hf_2O_7$ were prepared by conventional solid state reaction. Stoichiometric quantities of the starting materials, Pr_6O_{11} (Chempur, 99.999%) and HfO_2 (Chempur, 99.95%), were mixed, ground and heated to 1300 °C for 10 h and 1550 °C for 10 h with intermediate grinding. The synthesized powder was thoroughly reground and then isostatically pressed into cylindrical rods (6–8 mm in diameter and about 60–70 mm long). The resulting rods were sintered for several days in air at 1450 °C in preparation for crystal growth experiments.

Single crystals of $Pr_2Hf_2O_7$ were grown by the floating-zone technique using a four-mirror xenon arc lamp optical image furnace (CSI FZ-T-12000-X_VI-VP, Crystal Systems, Inc., Japan). The growths were performed in high purity argon at a pressure of ∼2 bars, using a growth rate of 18 mm h^{-1}. The feed and the seed rods were counter-rotated at around ∼20–30 rpm. Initially, a crystal boule of $Pr_2Zr_2O_7$ was used as seed and once good quality crystals of $Pr_2Hf_2O_7$ were obtained, the subsequent growths were carried out using crystal boules of $Pr_2Hf_2O_7$ as seeds.

Powder x-ray diffraction experiments were carried out at the Swiss Light Source (SLS) using the MS beamline (powder station) [47]. A diffraction pattern of the $Pr_2Hf_2O_7$ polycrystalline material (the starting material for the growth) was measured in a quartz capillary ($\phi = 0.1$ mm) with the Debye–Scherrer geometry and a multistrip MYTHEN II detector. The incident beam had an energy of ∼22 keV ($\lambda = 0.564\,941$ Å) and the diffracted beams were measured up to 60° 2θ, with a step size of ∼0.0036° 2θ. Powder neutron diffraction experiments were carried out on the starting polycrystalline material at the Swiss Spallation Neutron Source (SINQ) using the HRPT diffractometer ($\lambda = 1.155$ Å). Diffraction was measured between 5 and 162° 2θ, with a step size of 0.05° in 2θ, in a standard 'orange' helium cryostat. A joint Rietveld [48] refinement with equal weighting factors for the synchrotron and neutron data was performed using the FULLPROF software suite [49]. The instrumental resolution functions were determined experimentally from the measurements of small linewidth standards. A total of 23 parameters were refined: two sets of parameters independently refined for the two diffraction patterns (scale factors, zero-shifts, lattice parameter and sample contributions to the peak shapes), and 12 parameters defining the structural model (x coordinate of the 48f oxygen atom, anisotropic displacement parameters of all atoms and occupancy factors of three atomic positions).

In addition to the powder synchrotron x-ray diffraction pattern measured on the starting polycrystalline material, a measurement was also performed on a sample obtained by grinding a tiny crystal fragment from the middle of a single crystal. The drawbacks of using a powdered crystal fragment were the small amount of the resulting powder and the difficulty of grinding the crystal sample into very fine particles. The aforementioned factors hindered the realization of a full Rietveld analysis, because of insufficient powder averaging and poorly modelled lineshapes. Instead, these data were analyzed by a Le Bail decomposition [50] that was good enough to provide a precise estimate of the lattice parameter. The agreement factors for the refinement of the powder diffraction data given in the manuscript are defined in [51].

A Laue x-ray imaging system with a Photonic-Science Laue camera was used to investigate the quality of the crystal boules and orient single-crystal samples for selected experiments. A rectangular prism-shaped sample with dimensions of $2.73 \times 1.81 \times 1.96$ mm^3 was cut from the $Pr_2Hf_2O_7$ boule for magnetization measurements. The sample was cut so that the [1 1 0] (rhombic) and [0 0 1] (tetragonal) directions would be perpendicular to the faces of the rectangular prism. The demagnetizing factors were calculated using expressions derived by Aharoni [52].

Magnetization measurements were carried out using a Quantum Design Magnetic Property Measurement System MPMS-5S superconducting quantum interference device (SQUID) magnetometer, together with an i-Quantum ^{3}He insert. The magnetic susceptibility, which is equal to the magnetization M divided by the magnetic field H in the linear field regime, was evaluated as a function of temperature in a constant applied magnetic field of 1 kOe from 0.5 to 300 K. Magnetization measurements were also performed as a function of magnetic field up to 70 kOe directed along specific crystallographic axes at various temperatures.

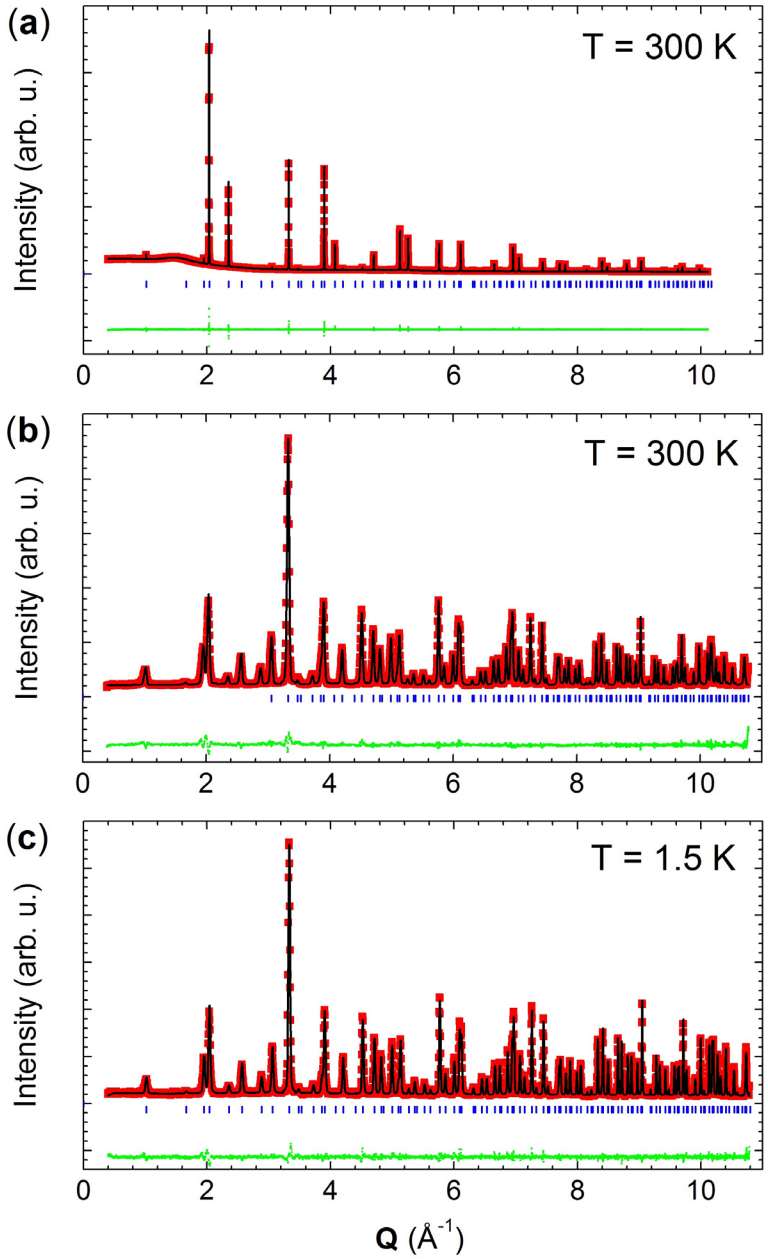

Figure 1. Rietveld refinement of powder: (a) synchrotron x-ray and (b), (c) neutron diffraction data collected at 300 K ((a) and (b)) and 1.5 K ((c)). Red, black and green represent the experimental data, the fit and the difference between the data and the fit respectively, while the blue ticks indicate the Bragg positions. The incident wavelengths are $\lambda = 0.621\,418$ Å ((a)) and $\lambda = 1.155$ Å ((b) and (c)). Patterns (a) and (b) are jointly refined against the common structural model given in table 1. The low-temperature structure corresponding to pattern (c) is presented in table 2. Conventional Rietveld factors for pattern (a) (%): $R_P = 1.70$; $R_{WP} = 2.04$; $R_{Bragg} = 2.66$; and $R_F = 7.45$. Conventional Rietveld factors for pattern (b) (%): $R_P = 3.88$; $R_{WP} = 5.19$; $R_{Bragg} = 4.24$; and $R_F = 2.58$. Conventional Rietveld factors for pattern (c) (%): $R_P = 3.88$; $R_{WP} = 5.19$; $R_{Bragg} = 3.91$; and $R_F = 2.55$.

3. Results and discussion

3.1. Crystal chemistry

Firstly, we investigated the crystal structure of $Pr_2Hf_2O_7$ in detail in order to confirm the relevance of this material as a model pyrochlore magnet. We used the polycrystalline sample prepared as the starting material for the crystal growth for these experiments. Diffraction patterns were measured using synchrotron x-ray (figure 1(a)) and neutron (figure 1(b)) radiation and refined together against the pyrochlore structure (space group $Fd\bar{3}m$, origin choice 2). The Rietveld procedure converges rapidly and the conventional agreement factors for Rietveld refinements [51] are $R_{WP} = 2.04$ and $R_{Bragg} = 2.66$ and $R_{WP} = 5.19$ and $R_{Bragg} = 4.24$, respectively for the synchrotron x-ray and neutron patterns at 300 K.

The joint refinement provides a complete description of the room-temperature crystal structure: a precise lattice parameter, bond distances/angles and anisotropic displacement parameters (ADPs), as well as a certain degree of sensitivity to the chemical composition thanks to the strong contrast in the

Table 1. Structural parameters for a polycrystalline sample of $Pr_2Hf_2O_7$ determined from a joint Rietveld refinement of synchrotron x-ray and neutron diffraction data measured at 300 K (space group $Fd\bar{3}m$, origin choice 2).

$T = 300$ K	x	y	z	Occupancy
Pr (16*d*)	0.5	0.5	0.5	0.994(12)
Hf (16*c*)	0	0	0	1
O (48*f*)	0.375	0.375	0.375	1.024(15)
O′ (8*b*)	0.332 47(7)	0.125	0.125	1.012(27)

ADPs in Å^2:	U_{11}	U_{22}	U_{33}	U_{12}	U_{13}	U_{23}
Pr (16*d*)	0.007 02	0.007 02	0.007 02	−0.000 84	−0.000 84	−0.000 84
Hf (16*c*)	0.003 55	0.003 55	0.003 55	0.000 15	0.000 15	0.000 15
O (48*f*)	0.009 66	0.007 12	0.007 12	0	0	0.002 69
O′ (8*b*)	0.006 65	0.006 65	0.006 65	0	0	0

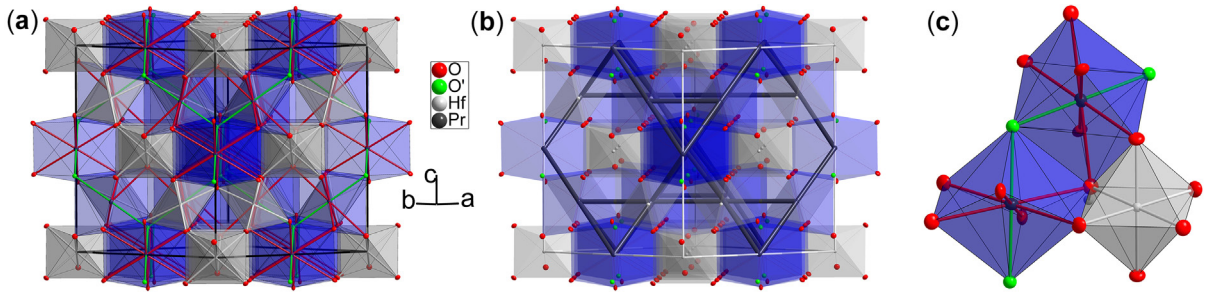

Figure 2. Crystal structure of $Pr_2Hf_2O_7$ obtained from the joint Rietveld refinement of synchrotron x-ray and neutron data measured at room temperature, $Fd\bar{3}m$, origin choice 2. In (a) the cell edges are drawn in black, and we emphasize the Pr–O (red), Pr–O′ (green) and Hf–O (grey) bonds. Blue and grey polyhedra show the oxygen scalenohedra and octahedra around the Pr^{3+} and Hf^{4+} cations, respectively. In (b) the cell edges are drawn in white and we emphasize the magnetic pyrochlore lattice of Pr^{3+} cations (in black). Panel (c) shows the local coordination around the two metals and the connection between the polyhedra.

neutron scattering lengths ($b_{Pr} = 4.58(5)$ fm, $b_{Hf} = 7.77(14)$ fm and $b_O = 5.805(4)$ fm). The results are summarized in table 1 and are in good agreement with previously published data [53, 54]. The resulting crystal structure at 300 K is shown in figure 2. The lattice parameter obtained from the powder synchrotron x-ray data is 10.684 11(2) Å. The value of the atomic coordinate x for the oxygen atom O(48*f*) is 0.332 47(7), in the range of the typical values for $A_2B_2O_7$ compounds [4]. The Pr–O(48*f*) bond length is 2.6016(6) Å, close to the sum of the ionic radii (∼2.66 Å), while the Pr–O′(8*b*) bond (pointing along the local ⟨1 1 1⟩ direction) has a length of 2.312 697(6) Å, which is markedly shorter than the 2.66 Å, as usually observed in rare-earth pyrochlores. Attempts to refine antisite cation disorder and oxygen Frenkel disorder did not provide evidence for any deviation from a perfectly ordered pyrochlore structure.

The joint refinement can also be used to retrieve information concerning the composition of the sample. Three of the four occupancy factors were refined in order to avoid total correlation with the scale factor. The refined chemical occupancies remain very close to unity (see table 1). Given this result, it is reasonable to assume a stoichiometric formula $Pr_2Hf_2O_7$ for our polycrystalline material.

Finally, we also collected a powder neutron diffraction pattern of $Pr_2Hf_2O_7$ at 1.5 K in order to determine values for the bond distances and angles that are relevant for the low-temperature superexchange pathways, and to check for structural distortions that may affect the magnetism of the non-Kramers Pr^{3+} ions. The crystal structure maintained its cubic symmetry at 1.5 K, where the lattice ($a = 10.665\,64(5)$ Å) contracted by about 1.5% compared to its value at 300 K ($a = 10.681\,89(5)$ Å, obtained from the refinement of the neutron diffraction pattern). The results of the refinement at 1.5 K (which is presented in figure 1(c)) are summarized in table 2. At 1.5 K the Pr–O(48*f*) bond length is 2.5937(6) Å and the Pr–O′ (8*b*) bond has a length of 2.309 179(6) Å.

3.2. Crystal growth

Crystals of $Pr_2Hf_2O_7$ were successfully grown by the floating-zone method, using similar growth conditions to those used for preparing $Pr_2Zr_2O_7$ crystal boules [38, 55]. One of the difficulties associated with the growth of praseodymium related compounds is the evaporation of Pr_2O_3 during the crystal growth process, which can cause a decrease in the Pr content in the single crystals [24, 38, 55]. This phenomena can be avoided by employing a high growth rate and performing the growth in a pressurized gas atmosphere (inside a quartz tube) to suppress the evaporation [38]. The crystal growth of $Pr_2Hf_2O_7$ was performed in high purity argon gas in order to facilitate the reduction of the Pr^{4+} ions to Pr^{3+} (see [38] and [39], and references therein). The $Pr_2Hf_2O_7$ crystals obtained were typically 5–7 mm in diameter and 60–85 mm long. The crystals developed well defined facets within the first few

Table 2. Structural parameters for a polycrystalline sample of $Pr_2Hf_2O_7$ obtained from a Rietveld refinement of powder neutron diffraction data measured at 1.5 K (space group $Fd\bar{3}m$, origin choice 2). The results are given assuming all the occupancy factors are equal to unity.

$T = 1.5$ K	x	y	z
Pr (16*d*)	0.5	0.5	0.5
Hf (16*c*)	0	0	0
O (48*f*)	0.375	0.375	0.375
O′ (8*b*)	0.333 01(7)	0.125	0.125

ADPs in Å^2:	U_{11}	U_{22}	U_{33}	U_{12}	U_{13}	U_{23}
Pr (16*d*)	0.003 34	0.003 34	0.003 34	0.000 62	0.000 62	0.000 62
Hf (16*c*)	0.001 16	0.001 16	0.001 16	−0.000 15	−0.000 15	−0.000 15
O (48*f*)	0.004 80	0.004 60	0.004 60	0	0	0.000 08
O′ (8*b*)	0.004 19	0.00419	0.004 19	0	0	0

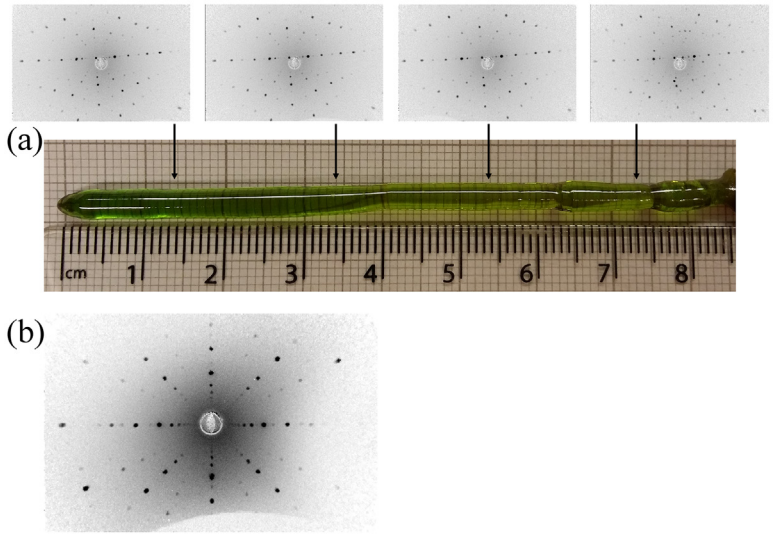

Figure 3. (a) Crystal of $Pr_2Hf_2O_7$ grown in a high purity argon atmosphere, at a pressure of ∼2 bars and a translation rate of 18 mm h^{-1}. Also shown above the image of the crystal are the Laue patterns of one of the facets, taken along the crystal length at ∼2 cm intervals, between the end (left) and the beginning (right) of the boule. The corresponding Laue patterns taken on the facet at 180 degrees are mirror images of these patterns. (b) Laue back reflection x-ray photograph of an aligned sample (showing the [0 0 1] orientation) used for the magnetic properties measurements discussed in this work.

millimetres of the growth and the boules obtained were free of any cracks. No deposition was observed on the quartz tube surrounding the sample during the growth process, suggesting that no evaporation occurred during any of the growths. All the praseodymium hafnate boules were transparent to light, with a bright green colour. A photograph of an as-grown crystal of $Pr_2Hf_2O_7$ is shown in figure 3(a). The crystal quality of the boules was investigated by Laue x-ray diffraction, and Laue photographs were taken along the length of the boule, on the faceted sides (see figure 3(a)). The Laue patterns were identical along the whole length of the faceted faces and, in most cases, the [1 1 0] direction was almost orthogonal to one of the facets. A Laue photograph taken on an aligned sample of $Pr_2Hf_2O_7$ used for magnetic properties measurements is shown in figure 3(b).

The powder synchrotron x-ray diffraction pattern of a ground fragment taken from the middle of the specimen shown in figure 3(a) was refined against the pyrochlore lattice (figure 4). The pattern matches very well with the cubic pyrochlore phase and no impurity peaks were present. Furthermore, the superlattice reflections that are the characteristic trademarks of the pyrochlore structure are clearly visible in the x-ray diffraction pattern. The lattice parameter (10.677 04(3) Å) was found to be slightly smaller than the value of 10.684 11(2) Å obtained at the same temperature and using the same method for our polycrystalline material (figure 1(a)). A difference in the value of the lattice parameter between the polycrystalline and single crystal samples has also been reported for the $Pr_2Zr_2O_7$ pyrochlore [38]. The smaller lattice parameter observed in the single crystals may be attributed to a very small difference in the stoichiometry of polycrystalline and single crystalline samples. We note, however, that we could not find evidence of different physical behaviour in the powder and single crystal samples, which appears to be consistent with the good agreement between our heat capacity data taken on single crystal samples [56] and other data recently reported for powder samples [57].

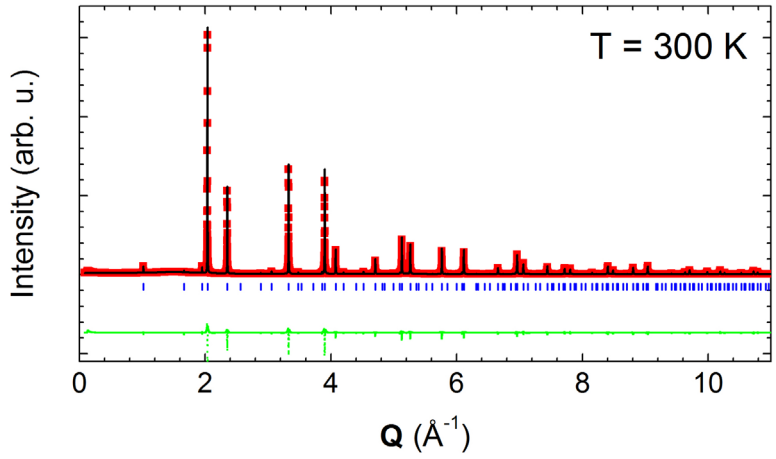

Figure 4. Powder synchrotron x-ray diffraction pattern collected on a ground crystal of $Pr_2Hf_2O_7$ at 300 K. The experimental profile (red) and a Le Bail decomposition (black) are shown, with the difference given in green. The Bragg positions are indicated by the blue ticks.

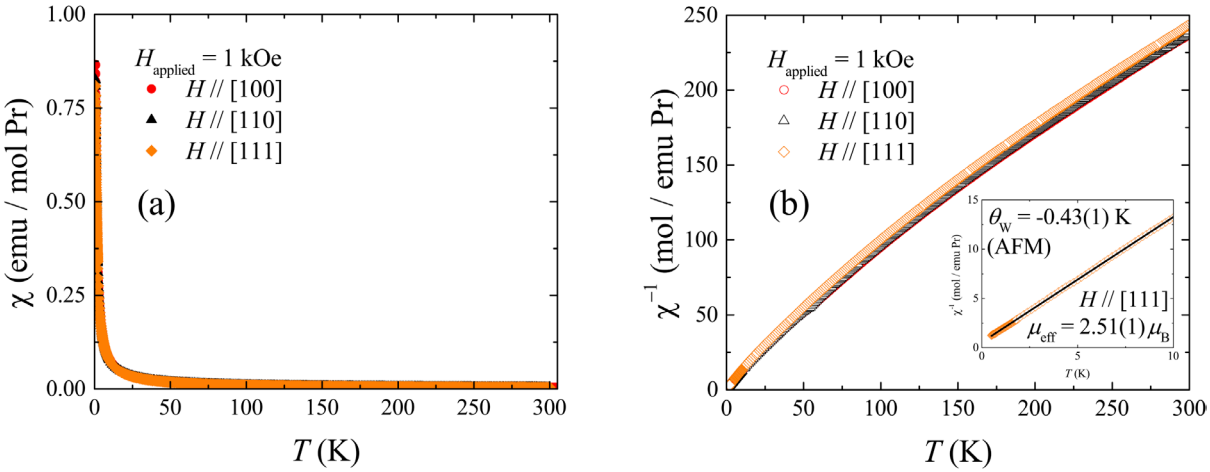

Figure 5. (a) Temperature dependence of the dc magnetic susceptibility, χ, versus T, in the temperature range 0.5–300 K for a crystal of $Pr_2Hf_2O_7$, with a magnetic field applied along the [1 0 0] (red), [1 1 0] (black) and [1 1 1] (orange) directions. (b) Temperature dependence of the reciprocal of the bulk dc susceptibility, χ^{-1} versus T, for a field applied along the three high symmetry directions. The inset shows χ^{-1} versus T and the linear fit (using the Curie–Weiss law) to the data in the temperature range 0.5–10 K for a magnetic field applied along the [1 1 1] direction.

3.3. Magnetic properties

Field-cooled (FC) and zero-field-cooled (ZFC) magnetization versus temperature data were collected on a $Pr_2Hf_2O_7$ rectangular prism-shaped single crystal aligned along the three high symmetry crystallographic directions ([1 0 0], [1 1 0] and [1 1 1]). The data were corrected for demagnetization effects [52] and the demagnetizing factors were found to be equal to $N = 0.38$, 0.35 and 0.25, respectively, where $H = H_{\text{applied}} - 4\pi MN$. Figure 5 shows the temperature dependence of the dc magnetic susceptibility, $\chi(T)$, and the reciprocal dc magnetic susceptibility $\chi^{-1}(T)$. The data measured along the different crystallographic axes in 1 kOe reveal a monotonic and highly isotropic (within experimental error) increase upon cooling from $T = 300$ to 0.5 K, and the absence of any anomaly that might indicate a magnetic transition. The $\chi^{-1}(T)$ data do not obey a Curie–Weiss law in the temperature range 0.5–300 K, although fits could be made over a reduced temperature range (0.5–10 K) (see figure 5(b) (inset)). It was found that the results of the fits depend on the exact temperature range over which the fit is performed. These results highlight the importance of investigating the crystal electric field (CEF) scheme in these systems. The crystal field splitting of Pr^{3+} in $Pr_2Hf_2O_7$ was determined and the results are described elsewhere [56]. In $Pr_2Hf_2O_7$ the first excited level is about 9.2 meV ∼107 K above the ground state doublet, meaning that information concerning the magnetic interactions can be deduced from a Curie–Weiss analysis well below this temperature. Accordingly, a fit of the magnetic susceptibility to a Curie–Weiss law was made in the temperature range from 0.5 to 10 K, yielding a Curie–Weiss temperature of $\theta_W = -0.43(1)$ K for the magnetic field applied along the [1 1 1] direction. This indicates the presence of antiferromagnetic interactions that are slightly weaker than in $Pr_2Zr_2O_7$, where $\theta_W = -1.4(1)$ K [27]. The Pr^{3+} effective moment is estimated to be $\mu_{\text{eff}} = 2.51(1)\mu_B$, a similar value to the one found in $Pr_2Zr_2O_7$ [27, 38]. The calculated values of the Curie–Weiss temperature θ_W, and of the effective moment μ_{eff}, are in

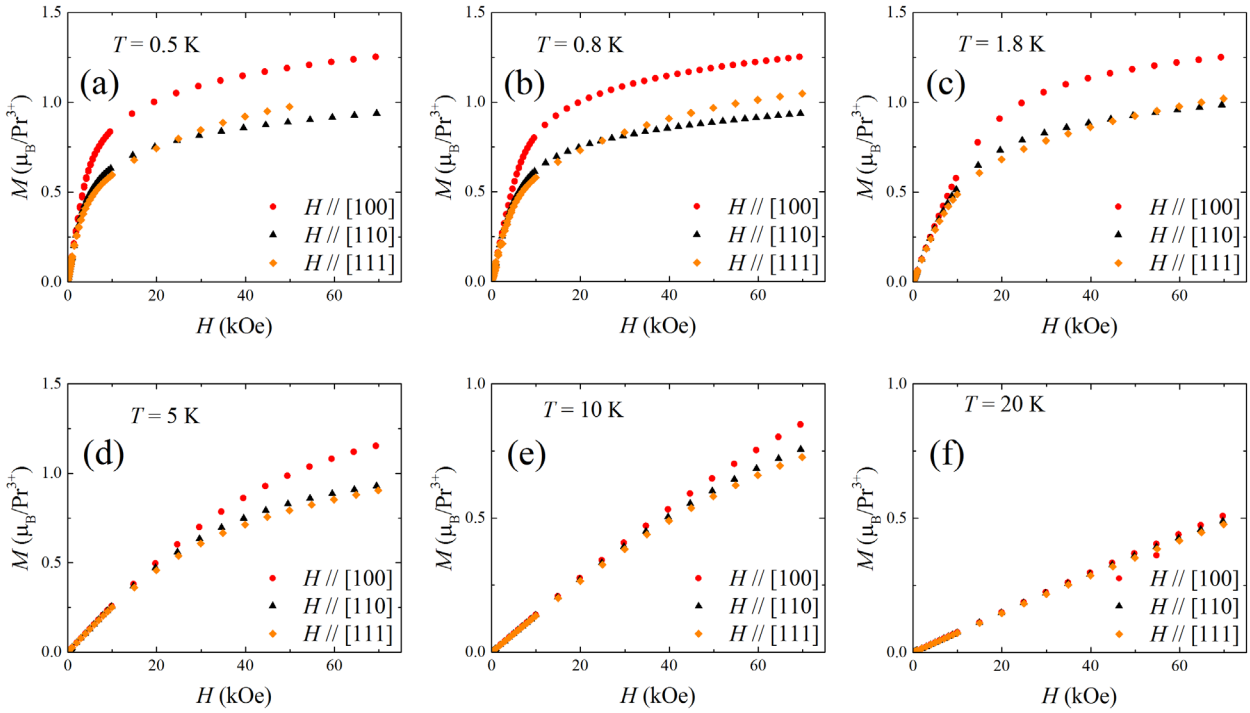

Figure 6. Isothermal magnetization (M) as a function of applied magnetic field (H) along the [1 0 0] (red), [1 1 0] (black) and [1 1 1] (orange) directions at temperatures of (a) 0.5, (b) 0.8, (c) 1.8, (d) 5, (e) 10 and (f) 20 K for a single-crystal of $Pr_2Hf_2O_7$.

agreement with those determined by detailed investigation of the low temperature magnetic properties of our $Pr_2Hf_2O_7$ crystals [56]. We note the apparent discrepancy between the negative Curie–Weiss temperature and the fact that the physics of Pr-based pyrochlores appears to be related to spin ice [27, 56, 58]. However, using inelastic neutron spectroscopy [58], it was recently established that in $Pr_2Zr_2O_7$ the parameters of the Hamiltonian for Pr-based pyrochlores [25] lead to a phase where quadrupolar correlations can overcome the antiferromagnetic exchange and account for the spin ice-like structure factor.

The magnetization measured along the three directions as a function of applied magnetic field $M(H)$ at various temperatures is shown in figure 6. The data collected at 1.8 K or below (see figures 6(a) and (b)) reveal a nonlinear response of the magnetization as the applied field increases. Furthermore, the field dependence of the magnetization appears to be reversible, with no hysteresis between the field-increasing and field-decreasing $M(H)$ curves. The magnetization measured with a magnetic field applied along the [1 0 0] direction is the highest in strong magnetic fields, whilst the [1 1 0] direction gives the lowest magnetization values. These results suggest similarities in terms of the local anisotropy of the magnetic moments between the $Pr_2Hf_2O_7$ pyrochlore and classical spin ice systems such as $Dy_2Ti_2O_7$ and $Ho_2Ti_2O_7$ [59, 60]. However, the values of the magnetic moments measured for the three crystallographic directions at the maximum applied field are smaller than the values of the expected saturated moments for a classic spin ice configuration [59]. A similar local ⟨111⟩ Ising behaviour was also observed in the related praseodymium zirconate pyrochlore, $Pr_2Zr_2O_7$ [27, 38, 43]. In $Pr_2Hf_2O_7$ the magnetization response is temperature dependent (see figures 6(a)–(f)), with the strongly anisotropic response only observed below about 10 K. Finally, we note the absence of evidence for a magnetization plateau developing in the $M(H)$ curve when the field is applied along the [1 1 1] direction, as opposed to observations made at much lower temperature [56]. The discrepancy only arises from the difference in temperature, because the apparent ferromagnetic correlations only appear below 0.5 K in this system [56].

4. Summary

We successfully prepared large, high quality single crystals of the novel frustrated pyrochlore magnet $Pr_2Hf_2O_7$ by the floating-zone technique, using a growth rate of 18 mm h^{-1} in a high purity argon atmosphere, at a pressure of ∼2 bars. Powder x-ray diffraction studies confirmed that the crystal boules were of a single-phase pyrochlore $Fd\bar{3}m$ structure. The quality of our $Pr_2Hf_2O_7$ single crystals appeared to be very high according to several criteria (colour homogeneity, absence of cracks, transparency, and quality and spatial homogeneity of the x-ray Laue diffraction patterns). The temperature dependence of the magnetic susceptibility measured in a low magnetic field showed an isotropic behaviour without any sign of long-range magnetic ordering down to 0.5 K. The field dependence of the isothermal magnetization revealed an anisotropic behaviour at low temperature, indicating a spin ice type of anisotropy. This magnetic response is similar to that seen in the related pyrochlore praseodymium zirconate, $Pr_2Zr_2O_7$. However, in contrast to the $Pr_2Zr_2O_7$ pyrochlore in which recent results point to the existence of a certain degree of disorder [58], the investigations performed on our $Pr_2Hf_2O_7$ crystals showed a structure with no cationic or

anionic deficiencies. A recent determination of the crystal field scheme in $Pr_2Hf_2O_7$ using neutron spectroscopy on polycrystalline samples [56] confirmed the nature of the anisotropy deduced for the bulk measurements presented here. The $Pr_2Hf_2O_7$ crystals produced are ideal for further investigation of the low temperature magnetism via neutron scattering techniques.

Acknowledgments

This work was supported by a grant from the EPSRC, UK (grant no. EP/M028771/1). The authors thank Mr Tom E Orton for valuable technical support. We acknowledge funding from the European Community's Seventh Framework Program (grant no. 290605, COFUND: PSI-FELLOW) and the Swiss National Science Foundation (grant nos 200021_138018 and 200020_162626). The neutron scattering experiments were carried out at the continuous spallation neutron source SINQ at the Paul Scherrer Institut at Villigen PSI in Switzerland and at the Institut Laue Langevin in Grenoble, France. The synchrotron powder x-ray diffraction measurements were carried out at the Materials Science beamline X04SA of the Swiss Light Source (SLS) at the Paul Scherrer Institut at Villigen PSI in Switzerland (Mesquik proposal 20161687).

References

[1] Blöte H W J, Wielinga R F and Huiskamp W J 1969 *Physica* **43** 549–68
[2] Bramwell S T and Gingras M J P 2001 *Science* **294** 1495–501
[3] Greedan J E 2001 *J. Mater. Chem.* **11** 37–53
[4] Gardner J S, Gingras M J P and Greedan J E 2010 *Rev. Mod. Phys.* **82** 53–107
[5] Malkin B Z, Lummen T T A, van Loosdrecht P H M, Dhalenne G and Zakirov A R 2010 *J. Phys.: Condens. Matter* **22** 276003
[6] Petrenko O A, Lees M R and Balakrishnan G 2011 *J. Phys.: Condens. Matter* **23** 164218
[7] Gingras M J P and McClarty P A 2014 *Rep. Prog. Phys.* **77** 056501
[8] Subramanian M A, Aravamudan G and Rao G V S 1983 *Prog. Solid State Chem.* **15** 55–143
[9] Harris M J, Bramwell S T, McMorrow D F, Zeiske T and Godfrey K W 1997 *Phys. Rev. Lett.* **79** 2554–7
[10] Bramwell S T *et al* 2001 *Phys. Rev. Lett.* **87** 047205
[11] Henley C L 2010 *Annu. Rev. Condens. Matter Phys.* **1** 179–210
[12] Fennell T, Deen P P, Wildes A R, Schmalzl K, Prabhakaran D, Boothroyd A T, Aldus R J, McMorrow D F and Bramwell S T 2009 *Science* **326** 415–7
[13] Castelnovo C, Moessner R and Sondhi S L 2008 *Nature* **451** 42–5
[14] Castelnovo C, Moessner R and Sondhi S L 2012 *Annu. Rev. Condens. Matter Phys.* **3** 35–55
[15] Greedan J, Sato M, Yan X and Razavi F S 1986 *Solid State Commun.* **59** 895–7
[16] Gaulin B D, Reimers J N, Mason T E, Greedan J E and Tun Z 1992 *Phys. Rev. Lett.* **69** 3244–7
[17] Zhou H D, Wiebe C R, Harter A, Dalal N S and Gardner J S 2008 *J. Phys.: Condens. Matter* **20** 325201
[18] Ross K A, Savary L, Gaulin B D and Balents L 2011 *Phys. Rev.* X **1** 021002
[19] Chang L J, Onoda S, Su Y, Kao Y J, Tsuei K D, Yasui Y, Kakurai K and Lees M R 2012 *Nat. Commun.* **3** 992
[20] Applegate R, Hayre N R, Singh R R P, Lin T, Day A G R and Gingras M J P 2012 *Phys. Rev. Lett.* **109** 097205
[21] Robert J, Lhotel E, Remenyi G, Sahling S, Mirebeau I, Decorse C, Canals B and Petit S 2015 *Phys. Rev.* B **92** 064425
[22] Jaubert L D C, Benton O, Rau J G, Oitmaa J, Singh R R P, Shannon N and Gingras M J P 2015 *Phys. Rev. Lett.* **115** 267208
[23] Zhou H D, Wiebe C R, Janik J A, Balicas L, Yo Y J, Qiu Y, Copley J R D and Gardner J S 2008 *Phys. Rev. Lett.* **101** 227204
[24] Matsuhira K, Sekine C, Paulsen C, Wakeshima M, Hinatsu Y, Kitazawa T, Kiuchi Y, Hiroi Z and Takagi S 2009 *J. Phys.: Conf. Ser.* **145** 012031
[25] Onoda S and Tanaka Y 2010 *Phys. Rev. Lett.* **105** 047201
[26] Lee S, Onoda S and Balents L 2012 *Phys. Rev.* B **86** 104412
[27] Kimura K, Nakatsuji S, Wen J J, Broholm C, Stone M B, Nishibori E and Sawa H 2013 *Nat. Commun.* **4** 1934
[28] Sibille R, Lhotel E, Pomjakushin V, Baines C, Fennell T and Kenzelmann M 2015 *Phys. Rev. Lett.* **115** 097202
[29] Curnoe S H 2008 *Phys. Rev.* B **78** 094418
[30] Hermele M, Fisher M P A and Balents L 2004 *Phys. Rev.* B **69** 064404
[31] Benton O, Sikora O and Shannon N 2012 *Phys. Rev.* B **86** 075154
[32] Savary L and Balents L 2012 *Phys. Rev. Lett.* **108** 037202
[33] Balakrishnan G, Petrenko O A, Lees M R and Paul D M 1998 *J. Phys.: Condens. Matter* **10** L723
[34] Gardner J S, Gaulin B D and Paul D M 1998 *J. Cryst. Growth* **191** 740–5
[35] Prabhakaran D and Boothroyd A T 2011 *J. Cryst. Growth* **318** 1053–6
[36] Taguchi Y, Ohgushi K and Tokura Y 2002 *Phys. Rev.* B **65** 115102
[37] Kézsmárki I, Hanasaki N, Hashimoto D, Iguchi S, Taguchi Y, Miyasaka S and Tokura Y 2004 *Phys. Rev. Lett.* **93** 266401
[38] Ciomaga Hatnean M, Decorse C, Lees M R, Petrenko O A, Keeble D S and Balakrishnan G 2014 *Mater. Res. Express* **1** 026109
[39] Koohpayeh S M, Wen J J, Trump B A, Broholm C L and McQueen T M 2014 *J. Cryst. Growth* **402** 291–8
[40] Ciomaga Hatnean M, Lees M R and Balakrishnan G 2015 *J. Cryst. Growth* **418** 1–6
[41] Hanasaki N, Kinuhara M, Kézsmárki I, Iguchi S, Miyasaka S, Takeshita N, Terakura C, Takagi H and Tokura Y 2006 *Phys. Rev. Lett.* **96** 116403
[42] Kézsmárki I, Hanasaki N, Watanabe K, Iguchi S, Taguchi Y, Miyasaka S and Tokura Y 2006 *Phys. Rev.* B **73** 125122
[43] Kimura K, Nakatsuji S and Nugroho A A 2013 *J. Korean Phys. Soc.* **63** 719–21
[44] Ciomaga Hatnean M, Lees M R, Petrenko O A, Keeble D S, Balakrishnan G, Gutmann M J, Klekovkina V V and Malkin B Z 2015 *Phys. Rev.* B **91** 174416
[45] Chun J, Reuvekamp P G, Chen D, Lin C and Kremer R K 2015 *J. Mater. Chem.* C **3** 491–4
[46] Tokiwa Y, Ishikawa J J, Nakatsuji S and Gegenwart P 2014 *Nat. Mater.* **13** 356–9
[47] Willmott P R *et al* 2013 *J. Synchrotron Radiat.* **20** 667–82
[48] Rietveld H M 1969 *J. Appl. Crystallogr.* **2** 65–71
[49] Rodríguez-Carvajal J 1993 *Phys. B: Condens. Matter* **192** 55–69
[50] Le Bail A, Duroy H and Fourquet J L 1988 *Mater. Res. Bull.* **23** 447–52
[51] McCusker L B, Von Dreele R B, Cox D E, Louërd D and Scardie P 1999 *J. Appl. Crystallogr.* **32** 36–50

[52] Aharoni A 1998 *J. Appl. Phys.* **83** 3432–4
[53] Karthik C, Anderson T J, Gout D and Ubic R 2012 *J. Solid State Chem.* **194** 168–72
[54] Blanchard P E R, Liu S, Kennedy B J, Ling C D, Avdeev M, Aitken J B, Cowie B C C and Tadich A 2013 *J. Phys. Chem.* C **117** 2266–73
[55] Ciomaga Hatnean M, Decorse C, Lees M R, Petrenko O A and Balakrishnan G 2016 *Crystals* **6** 79
[56] Sibille R, Lhotel E, Ciomaga Hatnean M, Balakrishnan G, Fåk B, Fennell T and Kenzelmann M 2016 *Phys. Rev.* B **94** 024436
[57] Anand V K *et al* 2016 *Phys. Rev.* B **94** 144415
[58] Petit S *et al* 2016 *Phys. Rev.* B **94** 165153
[59] Fukazawa H, Melko R G, Higashinaka R, Maeno Y and Gingras M J P 2002 *Phys. Rev.* B **65** 054410
[60] Petrenko O A, Lees M R and Balakrishnan G 2003 *Phys. Rev.* B **68** 012406